Atmospheric Research 339 (2026) 109062

Contents lists available at ScienceDirect

Atmospheric Research

journal homepage: www.elsevier.com/locate/atmosres

# Near-real time episode identification: Long-range transport of Canadian wildfire aerosol

M. Acton-Bond [a,b,1], S. Rimoldi [a,1], V. Bernardoni [a,b], L. Cadeo [a,b], G. Valli [a,b], C. Colombi [c], R. Cosenza [c], R. Vecchi [a,b,*]

[a] Department of Physics, Università degli Studi di Milano, Milan, 20133, Italy
[b] INFN-Milan, National Institute of Nuclear Physics, Milan 20133, Italy
[c] ARPA Lombardia, Regional Environmental Agency, Milan 20133, Italy

ARTICLE INFO

*Keywords:*
Absorption coefficient
Scattering coefficient
Aerosol sources
Aerosol typing
Episode identification
Canadian wildfires
Back trajectories

ABSTRACT

Air quality has significant impacts on human health, the environment and climate, with atmospheric aerosol playing a key role. As such, the development of methodologies for aerosol typing at a highly resolved time frame is of great value to monitoring networks as they can aid in identifying at a fast pace and at a fine time resolution which aerosol sources are present in peak events of particulate matter pollution. In this context, optical data can be exploited for fast aerosol typing purposes as instruments which measure absorption and scattering coefficients operate at a time resolution of up to minute time frames.

In this work, we refined a previously developed aerosol typing methodology, namely a hierarchical clustering of Absorption/Scattering Ångström Exponents, to identify which aerosol sources are responsible for peak absorption and scattering episodes. As a case-study for testing the methodology, a dataset collected in Milan (Italy) was used; it comprises one-month multi-wavelength absorption and scattering coefficients detected at ground-level with 15-min resolution.

The methodology proved to be effective in characterising the role of local sources in peak events and led to the identification of a long-range transport of Canadian wildfire aerosol which occurred in June 2025 and affected the whole of Europe including Milan.

## 1. Introduction

Atmospheric aerosol has been linked to effects on human health, and, by influencing the radiative balance between incoming and outgoing solar radiation, on the environment and climate (see e.g., WHO Global Air Quality Guidelines, 2021; IPCC, 2023). As such, developing and testing strategies for the identification of aerosol sources is of paramount importance for safeguarding air quality, human health and the environment.

Aerosol particles are emitted in the atmosphere through source-specific physical processes (e.g. fuel combustion, wood burning, dust resuspension, wildfires, …) and these source-specific emission processes determine source-characteristic particle sizes (e.g. few tens to hundreds of nanometres for high-temperature combustion, micrometres for mineral dust and sea spray, …), shapes (e.g. fractals, cuboids, spheres, …), and chemical compositions (see e.g., Rivas et al., 2020; Li et al., 2016; Calvo et al., 2013).

The size, shape, and complex refractive index (thus the chemical composition) of the emitted aerosol particles determine how they interact with light. As such, different aerosol sources have different optical properties with different source-specific wavelength dependences; thus, by exploiting these optical quantities, namely the

* Corresponding author.
*E-mail address:* roberta.vecchi@unimi.it (R. Vecchi).
[1] shared first authorship

https://doi.org/10.1016/j.atmosres.2026.109062
Received 29 January 2026; Received in revised form 8 April 2026; Accepted 30 April 2026
Available online 4 May 2026

wavelength dependence of light-absorption and light-scattering coefficient data, information on the presence of certain aerosol sources can be retrieved (see e.g., Cazorla et al., 2013; Valentini et al., 2020).

Instruments that quantify atmospheric aerosol absorption or scattering coefficients at different wavelengths - e.g. the aethalometer (Drinovec et al., 2015) and integrated polar nephelometers (Müller et al., 2011) - are often found in both air-quality and research monitoring stations (e.g., Regional Environmental Agencies and the ACTRIS network (Aerosols, Clouds, and Trace Gas Research Infrastructure, https://www.actris.eu/)).

For urban sites, ground-based in-situ information for both absorption and scattering coefficients is still fairly limited (see e.g., Romano et al., 2019; Rimoldi et al., 2026; and literature therein); however, the new *Directive (EU) 2024/2881* (https://eur-lex.europa.eu/eli/dir/2024/2881/oj/eng) on air-quality monitoring has made black carbon (BC) measurements mandatory and, as "black" refers to the property with which light is absorbed by particles, only optical data can give a meaningful measure of this still ill-defined substance (see e.g., Petzold et al., 2013; and literature reported therein), thus invigorating the importance of available absorption coefficient data.

Despite scattering coefficient data is not strictly mandatory, as far as aerosol optics is concerned, the combined availability of multi-wavelength absorption coefficient and scattering coefficient data makes way for the development of more encompassing approaches than other models found in the literature which exploit optical data from in-situ ground-based measurements, as these consider only absorption coefficient data and are based on strong assumptions on the wavelength dependence of the absorption coefficient and the number of acting sources, see e.g. the aethalometer model (Sandradewi et al., 2008) and the MWAA model (Bernardoni et al., 2017). Indeed, in the literature, the Ångström classification matrix, i.e. the Scattering and Absorption Ångström exponents SAE and AAE scatterplot (see section 2.3 for their definition), is subdivided in regions corresponding to different aerosol types (see, e.g., Cazorla et al., 2013; Cappa et al., 2016) and has been widely used for aerosol typing purposes also for monitoring sites in the Mediterranean Basin (see, e.g., Ealo et al., 2016; Romano et al., 2019; Kaskaoutis et al., 2021).

In Rimoldi et al. (2026), we proposed a simple methodology which exploits atmospheric aerosol absorption and scattering coefficient data for near-real time aerosol typing (see section 2 for the full description of the methodology). This methodology again exploits the Ångström exponents SAE and AAE without subdividing the classification matrix but by dividing the scattered data points through hierarchical clustering methodologies thus avoiding the use of preconceived AAE and SAE subregions which, in general, could vary from site to site.

In this work, the aim was to develop a methodology which could exploit absorption and scattering coefficient data to garner information on which aerosol types are responsible for peak absorption and scattering events. To this end, we refined the Rimoldi et al., 2026, methodology by using data at a higher time resolution than what previously done and by applying it to the highest absorption and scattering values. To test the methodology, we applied it to a case-study dataset comprising multi-wavelength absorption and scattering data measured in Milan, the largest city in the Po Valley, Northern Italy. This area is widely recognised as a pollution hotspot as the surrounding Alps and the Apennine Mountains create favourable conditions for the accumulation of aerosol particles (Vecchi et al., 2007); opposite, pollutants can be dispersed with strong katabatic winds and/or free troposphere intrusions unless the displacing air has already a high loading of particulate matter like during Saharan dust intrusion events and wildfire aerosol advection episodes (see e.g., Mira-Salama et al., 2008; Diémoz et al., 2025).

Once the aerosol types were identified through AAE-SAE clustering, their sources were assessed with additional information. Indeed, the newly refined methodology identified which local aerosol sources are responsible for peak absorption and scattering events and singled out a Saharan dust advection episode followed by a weeklong episode which was later confirmed to be a long-range transport of Canadian wildfire aerosol through back-trajectory data and news headlines, showcasing its effectiveness.

## 2. Methodology

### 2.1. The monitoring station

We applied the previously described methodology to a one-month (May 22nd to June 21st, 2025) multi-wavelength absorption and scattering coefficient high-time resolved dataset, which was made available for the Milano-Pascal monitoring station part of the monitoring network managed by the Regional Environmental Agency (ARPA Lombardia). It is an urban background station, i.e. it is not directly affected by local sources, and is located in Milan, Italy, (45.478° N, 9.231° E) near the campuses of two universities.

### 2.2. Instruments and data

The dataset here analysed is just taken as a case-study, well-suited to show the effectiveness of the proposed methodology in identifying aerosol types during peak events due to high resolution and data coverage. The dataset consisted of 1-min resolved absorption coefficient ($b_{abs}$) data at 7 wavelengths ($\lambda_{aeth}$ = 370, 470, 520, 590, 660, 880, and 950 nm) measured by an AE33 Aethalometer (Magee Scientific) and of scattering coefficient ($b_{sca}$) data at 3 wavelengths ($\lambda_{neph}$ = 450, 525, and 635 nm) obtained by the Aurora 3000 integrated nephelometer (Ecotech).

To account for the renowned limitations of both instruments (see e.g., Drinovec et al., 2015; Yus-Dìez et al., 2021; Müller et al., 2011), data reduction has been extensively reported in Rimoldi et al. (2026); briefly, aethalometer data were corrected with the ACTRIS (Aerosol, Clouds and Trace gases Research Infrastructure Network) recommended harmonisation factor and nephelometer data were treated following Müller et al. (2011) and the parameterisations reported therein.

After the corrections were applied, both absorption and scattering coefficient data were averaged at a timescale of 15 min. Data when instruments were performing self-calibrations were excluded from the averages. All 1-h slots when nephelometer zero checks were in progress (which was every day from midnight to 1 AM) were also excluded from the analysis.

One should note that the aethalometer and nephelometer instruments work at different wavelengths, thus the absorption coefficients of aethalometer wavelengths were corrected to the closest nephelometer wavelengths by power law fitting absorption coefficients (see Bernardoni et al., 2021, for details).

Local meteorological data was also available from a nearby ARPA station, which is less than 3 km away from the site.

### 2.3. The AAE-SAE clustering method

The clustering methodology, applicable whenever multi-wavelength absorption and scattering coefficient data is available, was originally developed in Rimoldi et al. (2026) and refined herein. Briefly, the chosen data for clustering are intensive optical parameters, namely the Absorption Ångström Exponent (AAE) and Scattering Ångström Exponent (SAE), defined as:

$$AAE = -\frac{\ln\left(\frac{b_{abs}(\lambda_1)}{b_{abs}(\lambda_2)}\right)}{\ln\left(\frac{\lambda_1}{\lambda_2}\right)} \quad (1)$$

$$SAE = -\frac{\ln\left(\frac{b_{sca}(\lambda_1)}{b_{sca}(\lambda_2)}\right)}{\ln\left(\frac{\lambda_1}{\lambda_2}\right)} \quad (2)$$

which can be easily computed from direct online ground-based measurements and are both exponents of power laws thus being directly comparable parameters.

The methodology applies the Ward clustering method, which, as per its solving algorithm, minimises the increase in the total within cluster error sum of squares at each clustering stage (see Everitt et al., 2011, for more details). It is important to note that AAE and SAE values are normalised to take a null mean and unity standard deviation before the clustering algorithm takes place as to not bias results in favour of the parameter which takes values in a wider range. Finally, the cluster analysis provides the the AAE-SAE couples associated with the dominance of a certain aerosol type. Further details are reported in Rimoldi et al. (2026).

In the literature, AAE values are often considered to be source specific (see e.g., Savadkoohi et al., 2025) and is oftentimes used to differentiate between BC, BrC and dust aerosol. On the other hand, SAE is used as size proxy for aerosol particles. As mentioned previously, aerosols of different origin have different optical properties and different wavelength dependences for absorption and scattering coefficient data. AAE and SAE quantify this wavelength dependence. As such, each obtained cluster is interpreted as that ensemble of data points when a particular aerosol source and/or type is optically dominating over other sources and/or types.

In this work, we refined the methodology by applying the same clustering algorithm to episodes, herein defined as those data points with highest absorption or scattering coefficient values, i.e. higher than their respective 95th percentile. This provides insights into which aerosol sources and/or types are responsible for peak events, which is useful information to monitoring networks and policy makers for the development of adequate abatement strategies.

Furthermore, the number of clusters is to be determined by the analysis, and it is not presupposed as other models do. Ideally, the clustering output should be suggested by mathematical parameters, e.g. through the Calinksi-Harabasz criterion (Calinski and Harabasz, 1974), and confirmed through physical interpretation.

## 3. Results and discussion

### 3.1. Absorption and scattering coefficient data

Environmental physics datasets often comprise variables with strong variability. Rises and falls of measured data can be due to sources activating (e.g., traffic, wood burning, dust resuspension, …), sinks (e.g., rain wash-out or fall-out, deposition, …), transformation processes (e.g. secondary formation), and atmospheric dynamics (e.g., dispersion and dilution with particle free air, stability and accumulation of pollutants in a shallow mixing layer) (Seinfeld and Pandis, 2006).

In Fig. 1, shown here as an example, one finds the absorption $b_{abs}$ and scattering $b_{sca}$ coefficients at 450 nm for the period from May 22nd to June 21st, 2025. In Fig. 2, one finds the corresponding AAE and SAE values calculated for the 450 nm and 635 nm wavelength pair.

Peak events can be identified for both absorption and scattering coefficient time plots. These are found both for brief periods (e.g., the sharp peak in May) and longer periods lasting days (e.g. the weeklong June scattering peaks).

Registering acute as well as broad in time absorption and scattering coefficient peaks, from a monitoring network's perspective, points to the need of finding an approach that can swiftly identify the origin of the measured signal. Indeed, knowing as fast as possible what caused the peak can greatly help local authorities take action to better safeguard air quality and/or can lead to the early identification of episodes which can be singled out and studied more in depth at a later stage.

Absorption and scattering coefficients represented in Fig. 1 give quantitative information on how much absorption and scattering due to aerosol particles was detected in our case-study. An abnormal peak can be observed in the data series, but it was not excluded from our analysis as it was reported by multiple instruments at once and occurred during an exceptional meteorological condition for the investigated site (wind speed higher than 10 m $s^{-1}$, intense precipitation, damages in the area due to tree and tiles falls, see Fig. S1 for meteorological data). Although this is interesting information on atmospheric optical properties, the represented data is not helpful in identifying aerosol types and their origin; opposite, the AAE-SAE analysis exploits the wavelength-dependence of the measured absorption and scattering signals and thus provides information on aerosol types.

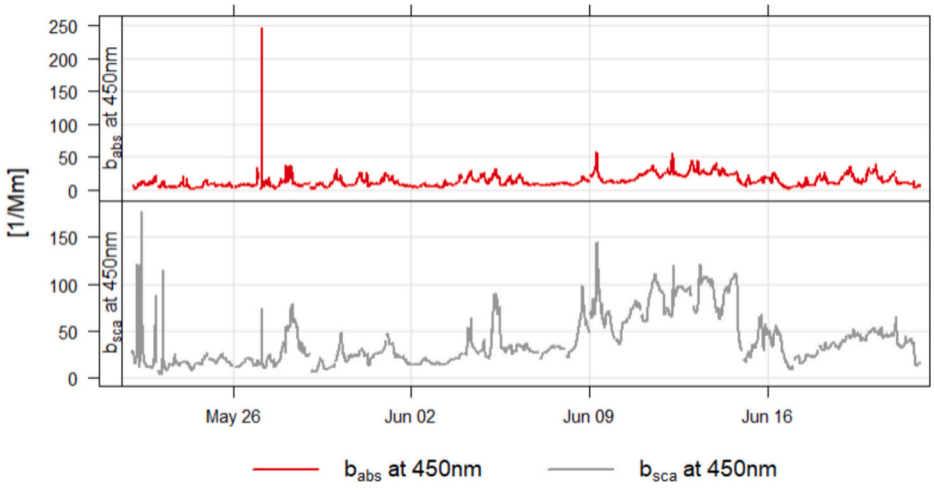


**Fig. 1.** Absorption and scattering coefficient at 450 nm from May 22nd to June 21st, 2025.

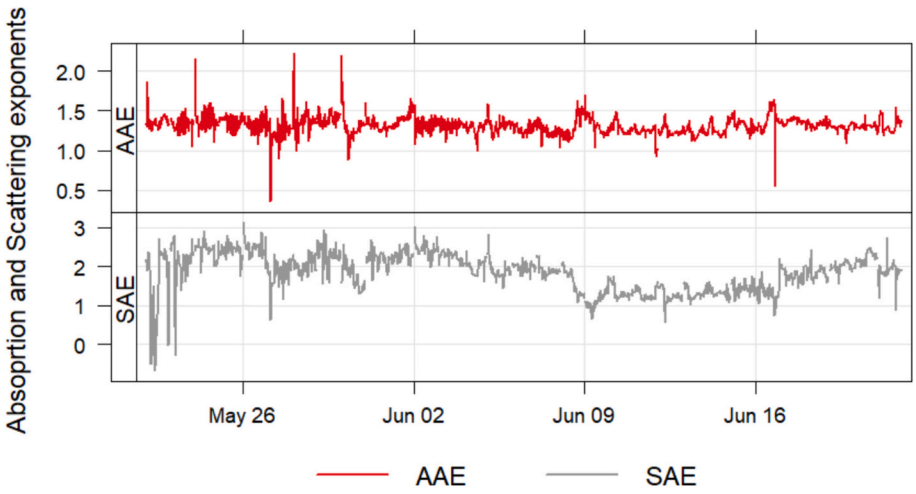


**Fig. 2.** AAE and SAE for the 450 nm and 635 nm wavelength pair from May 22nd to June 21st, 2025.

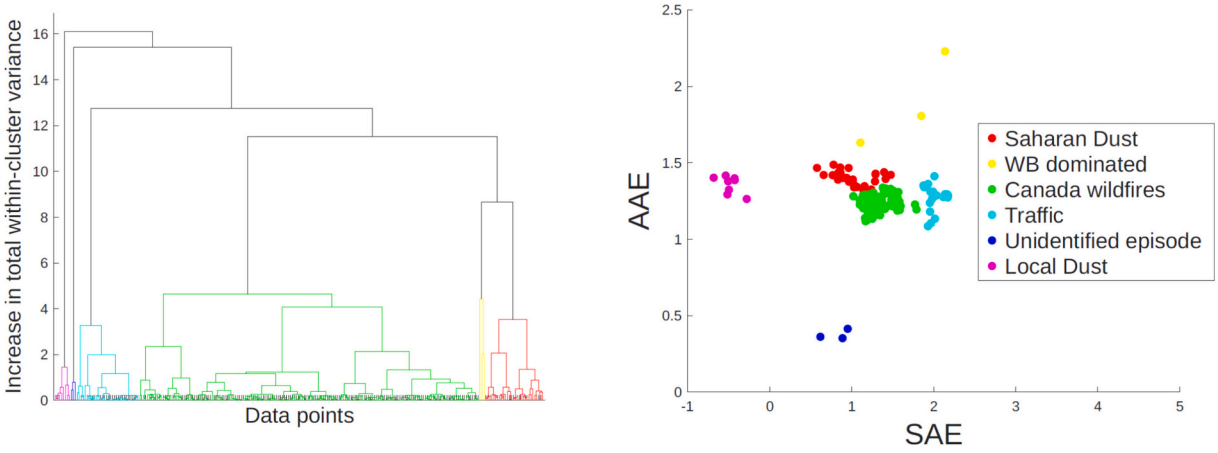


**Fig. 3.** (a) dendrogram and (b) AAE-SAE clusters of data with absorption or scattering coefficients at 450 nm over their respective 95th percentile.

In the following section we focus our attention on the highest absorption and scattering coefficients values together with their corresponding AAE and SAE values with the goal of typing aerosol in peak-concentration events.

### 3.2. Aerosol typing

Contrary to what previously done in Rimoldi et al. (2026), where the focus was aerosol typing using all data points from a long data series, in this paper, we focused on data when either absorption or scattering coefficients at 450 nm exceeded their respective 95th percentile. Data points respecting this condition are referred to as "episodes" and were analysed with the clustering method described in section 2.1 for aerosol typing in peak events. Because, scattering and absorption peaks are neither completely independent nor completely dependent from one another, a maximum of 10% and a minimum of 5% of the whole dataset can follow this request at once. In this work, approximately 8.5% of the whole available dataset was kept.

The clustering dendrogram and the AAE-SAE biplot are shown in Fig. 3a and Fig. 3b, respectively. The Calinksi-Harabasz criterion suggested the optimal number of clusters to be five which was then raised to six based on the physical interpretability of the solution as the wood burning WB dominated cluster separated from the Saharan dust cluster. The interpretation of the clusters was carried out by contemplating AAE and SAE values (see Fig. 3b for the AAE-SAE cluster plot), by considering their temporal activation in time (see Fig. 4 for their daily fractional contribution) and by considering atmospheric circulation and meteorology (see Fig. S1).

Clusters with high AAE values and SAE values of up to two can be ascribed to wood burning which is still widespread in the Po Valley for domestic heating purposes in autumn and winter (see e.g., Forello et al., 2019; and therein cited literature). May and June are warmer months and, as expected, the WB dominated cluster comprised only three episodes of 15-min averaged data, the origin of which might not be related to domestic heating but to other wood burning sources such as wood-burning ovens and grills.

The first half of the campaign, i.e. the last week of May and the first week of June, was less impacted by episodes compared to the following period. At this time of year atmospheric meteorology and dynamics frequently cleanse the Po Valley air; indeed, herein highest mixing layers (Vecchi et al., 2019), strong precipitations, and strong katabatic advection episodes can occur. The few episodes occurring in May were mainly found to be dust-dominated and traffic-derived aerosol peak events. Indeed, these clusters were identified following previous results reported in Rimoldi et al. (2026), where we showed that clusters with low SAE vales are linked to dust resuspension and clusters with SAE values around 2 and low AAE values (AAE $< 1.5$) indicate BC particles derived from liquid fuel combustion are those optically dominating over other aerosol types and/or sources.

The unidentified episode cluster arises from a very sharp peak of less than an hour for both absorption and scattering coefficients which occurred during the night of May 27th at around 3:00 AM. Low SAE and

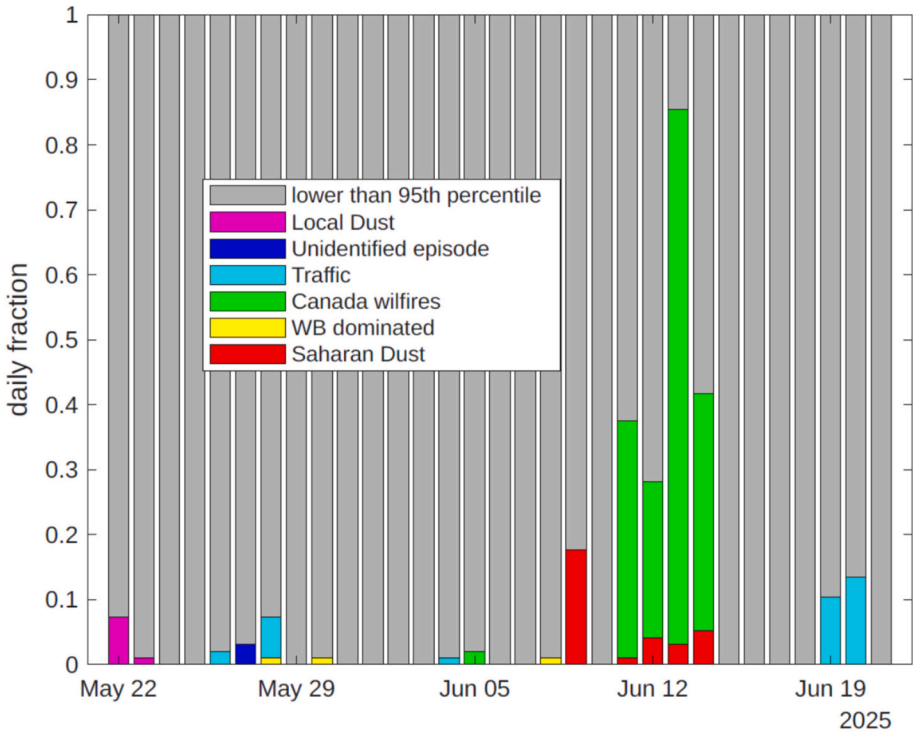


**Fig. 4.** May and June 2025 daily fractional cluster contribution for data with absorption or scattering coefficients at 450 nm over their respective 95th percentile.

AAE values suggested large absorbing particles were optically dominating during this brief period. Herein maximum gust speeds clocked in at 10.3 m $s^{-1}$, intense precipitation occurred reaching rainfall hourly cumulated values of 15 mm, local newspapers recorded tree fall near the monitoring site and many fire department calls because of loose roof tiles and flooded buildings (see Fig. S1 for meteorological data). The origin and cause of this peak remain largely unidentified which is the reason behind the corresponding cluster name. By applying the same episode methodology on a longer data series more quantitative information might be obtained.

June campaign days, on the other hand, were heavily impacted by episodes with two different clusters being the main contributors. High AAE values and low SAE values suggest mineral dust particles are present (see e.g., Valentini et al., 2020; Rimoldi et al., 2026) which is the reason for the aptly named Saharan dust cluster.

On June 13th, 82% of the data points surpassed the 95th percentile limit for absorption or scattering coefficient data. As better explained in the next section, these data points were associated to a cluster that was later ascribed to a long-range transport of Canadian wildfire aerosol.

**Table 1**
$PM_{10}$ and $PM_{2.5}$ concentration values i) of EU-imposed limits as of June 2025, ii) on June 13th, iii) averaged over the Canadian Wildfire episode from June 8th to June 16th and iv) averaged over all the other days in June.

| | EU-imposed mass concentration limit as of June 2025 | daily mass concentration of June 13th | mean mass concentration 8th–16th June | mean mass concentration of all other days |
|---|---|---|---|---|
| $PM_{2.5}$ | 25 μg/$m^3$ | 29 μg/$m^3$ | (19 ± 8) μg/$m^3$ | (10 ± 3) μg/$m^3$ |
| $PM_{10}$ | 50 μg/$m^3$ | 41 μg/$m^3$ | (30 ± 6) μg/$m^3$ | (15 ± 5) μg/$m^3$ |

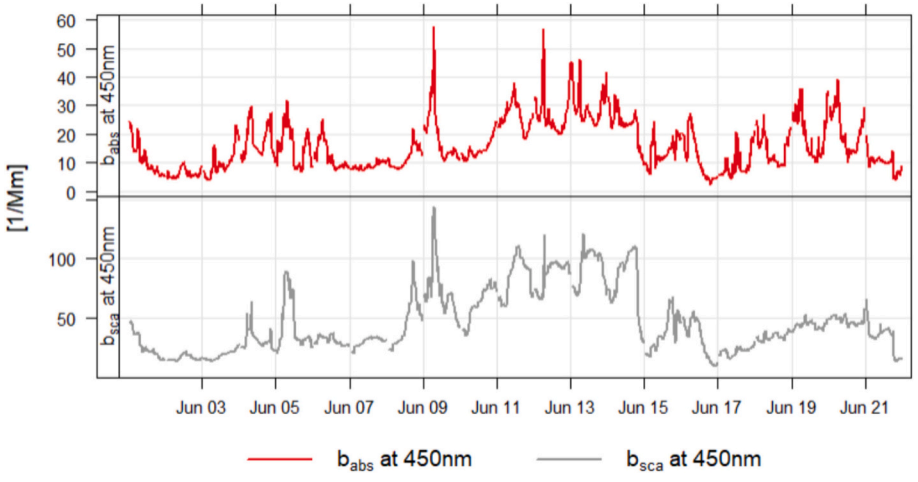


**Fig. 5.** 15-min averaged absorption and scattering coefficient at the 450 nm during June campaign days.

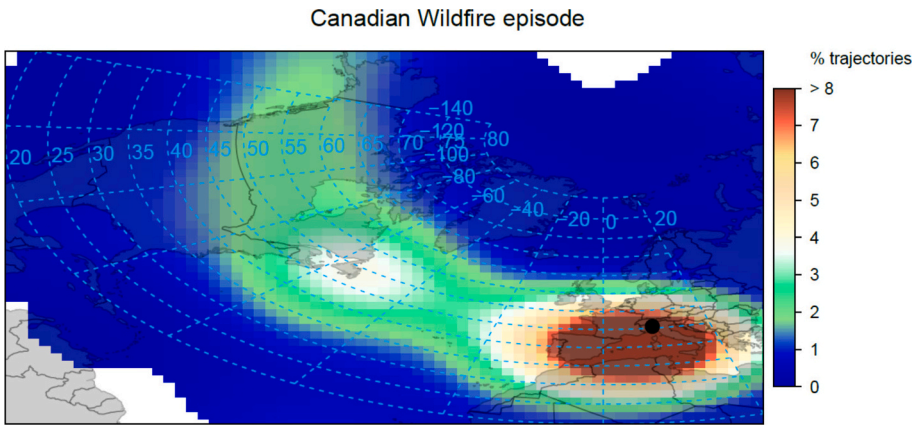


**Fig. 6.** percentage of back-trajectories associated to the Canadian wildfire episode from the 8th to the 16th of June. Bins span 5° longitudinally and latitudinally.

### 3.3. *Canadian wildfires and Saharan dust advection*

In Fig. 5, one finds absorption and scattering coefficients shown for the period from June 6th to June 21st, 2025. From June 8th to June 16th scattering data showed higher values at the same time as increased PM daily mass concentrations (see Table 1) which were almost double the mean value of the other June days. On June 13th PM mass concentrations reached their maximum value and were 41 μg/m$^3$ and 29 μg/m$^3$ for $PM_{10}$ and $PM_{2.5}$, respectively. Herein, $PM_{2.5}$ daily concentrations were higher than the EU-imposed daily limit of 25 μg/m$^3$ highlighting the relevance of having fast information, like optical data, in monitoring networks so Regional Environmental Agencies can act swiftly if need be and alert citizens in peak-concentration events.

By zooming in on the mentioned period (see Fig. S3), scattering peaks were found during the daytime when mixing layers are usually at their highest suggesting that it was the high-altitude air, thus synoptic atmospheric circulation, that was heavily polluted. This was also confirmed by the increase and strong modulation of ground-level radon ($^{222}$Rn) activity concentrations – here used as a marker for atmospheric dilution conditions (see Vecchi et al., 2019, for details on the measuring site and procedure). Furthermore, in Fig. 4, from June 11th to June 14th more than 20% of data points in a day were higher than the 95th percentile of the whole period and more than 20% of hours were associated to the green and red clusters.

The same AAE-SAE clustering methodology was applied to AAE and SAE data with absorption and scattering coefficients at 450 nm higher than their respective 75th percentile (results are shown in Fig. S2). Analogous results were found and show that the whole June 8th to June 16th period can be largely described by the same two above mentioned clusters. One should note that these analogous results show the methodology to be robust and stable when choosing different percentile limits, i.e. even if one includes more/less data points in the analysis.

To explain the origin of both clusters, back-trajectory analyses were carried out following the air parcel at half the height of the Planet Boundary Layer (PBL) back in time for 600 h (25 days) every hour from June 1st to June 21st with the NOAA (National Oceanic and Atmospheric Administration) - HYSPLIT model (Stein et al., 2015; Rolph et al., 2017). GDAS (Global Data Assimilation System) meteorological data with a 1°x1° longitude-latitude grid resolution were used as input to the HYSPLIT model.

In Fig. 6, one finds frequency back-trajectory data for all hours from June 8th to June 16th. Air was preferentially flying in directly from Canada where wildfires (primarily in Manitoba, Ontario, and Saskatchewan) were active throughout May (see the following link https://atmosphere.copernicus.eu/2025-sees-intense-wildfire-year-northern-hemisphere, last accessed on the 31st of March 2026, for an animation of the May–June 2025 Canadian wildfire plume). Trans-Continental atmospheric circulation picked up the wildfire-aerosol polluted air and transported it to the doorstep of Europe in the first days of June and throughout Europe in the weeks thereafter. For these reasons, this cluster was associated to the long-range transport of Canadian wildfire aerosol. AAE values for the Canadian wildfire cluster were lower than ones expect for biomass burning, as AAE values decrease as the distance from the biomass-burning site increases (see e.g., Diapouli et al., 2014; and literature therein) possibly due to brown carbon bleaching due to photo-oxidation processes being accentuated at shorter wavelengths compared to longer one (Sumlin et al., 2017), whilst SAE values were intermediate (see Rimoldi et al., 2026, for typical values in Milan) as both coarse and finer fractions of aerosol can be picked up in wildfires (Portin et al., 2012). Some data points had

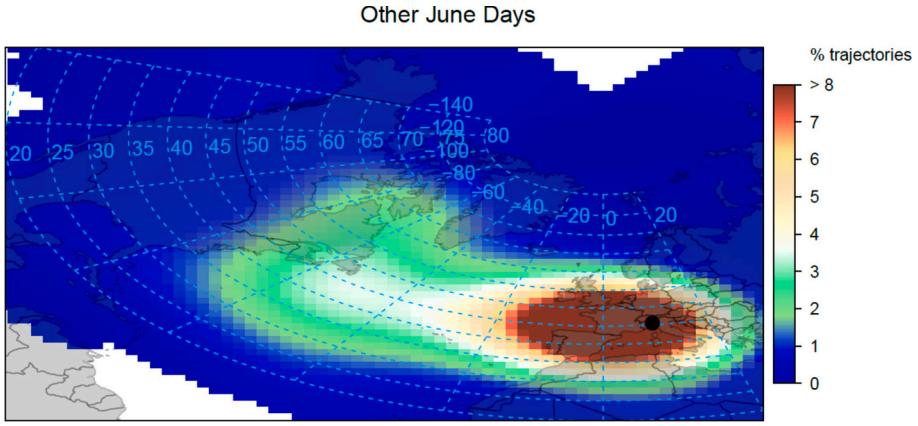


**Fig. 7.** percentage of back-trajectories from June 1st to June 7th and from June 17th to June 21st. Bins span 5° longitudinally and latitudinally.

lower SAE values and higher AAE values than the Canadian wildfire cluster and were associated to a different cluster ascribed to Saharan dust. Indeed, as shown in Fig. 6 some back trajectories passed through the northwestern tip of the Mediterranean African coast suggesting a mineral dust origin for the aptly named Saharan dust cluster. Copernicus CAMS simulations (https://www.copernicus.eu/en/news/news/observer-air-quality-challenges-2025-europes-summer-smoke-dust-and-ozone#:~:text=Throughout%20June%2C%20several%20Saharan%20dust last accessed on December 19th, 2025) confirmed Saharan dust was transported to Europe during June days.

In Fig. 7, one finds percentages of June back-trajectory data not associated to the Canadian wildfire episode, i.e. from June 1st to June 7th and from June 17th to June 21st. Indeed, although air is still flowing into Europe through the easternmost tip of Canada it does so without a clearcut direction as is the case for the days of Fig. 6.

## 4. Conclusions

In this work, the focus was to type aerosol in episodes with peak absorption and scattering coefficient values measured at ground-level monitoring stations. We refined a previously developed hierarchical clustering algorithm, which exploits multi-wavelength absorption and scattering coefficient data to garner information on acting aerosol types and sources, by limiting the analysis to episodes, i.e. data points with absorption or scattering coefficients higher than their respective 95th percentiles. Compared to other aerosol typing methods, here a-priori ranges of optical values (e.g., site-specific AAE-SAE intervals) are not needed to identify aerosol types. This makes the methodology simple in its implementation and generally applicable at any site.

We showed the effectiveness of the methodology when applied to a one-month dataset of 15-min averaged absorption and scattering coefficients in Milan, Italy, used here as a case-study. Six aerosol types were found as contributors to high absorption and scattering coefficient events, four of which were ascribed to local sources through their AAE and SAE value, i.e. dust-resuspension, wood burning-dominated and traffic-derived aerosol and a sharp peak during a thunderstorm. Two additional clusters, which were clearly active in a relatively brief period of June, were identified as pertaining to a long-range transport of Canadian wildfire aerosol and to Saharan dust advection which was confirmed through HYSPLIT back-trajectory data analyses.

In the vision for prompt air quality data assessment and interpretation, this simple clustering method was confirmed to be effective in exploiting light absorption and scattering data for preliminary and fast episode identification, as well as typing local sources appropriately, in peak absorption and scattering events. The simplicity of the approach and the fast response of optical instruments make this clustering method implementable in monitoring networks and an excellent candidate for near-real time aerosol typing.

## CRediT authorship contribution statement

**M. Acton-Bond:** Writing – original draft, Methodology, Formal analysis, Data curation, Conceptualization. **S. Rimoldi:** Writing – original draft, Validation, Methodology, Formal analysis, Conceptualization. **V. Bernardoni:** Writing – review & editing, Supervision, Methodology. **L. Cadeo:** Writing – review & editing, Visualization, Validation. **G. Valli:** Writing – review & editing, Visualization, Methodology. **C. Colombi:** Writing – review & editing, Resources, Investigation, Data curation. **R. Cosenza:** Writing – review & editing, Investigation, Data curation. **R. Vecchi:** Writing – review & editing, Writing – original draft, Supervision, Resources, Funding acquisition, Conceptualization.

## Funding

This research was partly funded by the project “One Health Action Hub: University Task Force for the resilience of territorial ecosystems”, Supported by Università degli Studi di Milano – PSR 2021 - GSA - Linea 6.

## Declaration of competing interest

The authors declare that they have no known competing financial interests or personal relationships that could have appeared to influence the work reported in this paper.

## Acknowledgements

The authors gratefully acknowledge the NOAA Air Resources Laboratory (ARL) for the provision of the HYSPLIT transport and dispersion model (https://www.ready.noaa.gov) used in this publication and ARPA Lombardia for data availability.

## Appendix A. Supplementary data

Supplementary data to this article can be found online at https://doi.org/10.1016/j.atmosres.2026.109062.

## Data availability

Data will be made available on request.

## References

Bernardoni, V., Pileci, R.E., Caponi, L., Massabò, D., 2017. The Multi-Wavelength Absorption Analyzer (MWAA) model as a tool for source and component apportionment based on aerosol absorption properties: application to samples collected in different environments. Atmosphere 8, 218. https://doi.org/10.3390/atmos8110218.

Bernardoni, V., Ferrero, L., Bolzacchini, E., Forello, A.C., Gregorič, A., Massabò, D., Mocnik, G., Prati, P., Rigler, M., Santagostini, L., Soldan, F., Valentini, S., Valli, G., Vecchi, R., 2021. Determination of Aethalometer multiple-scattering enhancement parameters and impact on source apportionment during the winter 2017/18 EMEP/ACTRIS/COLOSSAL campaign in Milan. Atmos. Meas. Tech. 14, 2919–2940. https://doi.org/10.5194/amt-14-2919-2021.

Calinski, T., Harabasz, J., 1974. A dendrite method for cluster analysis. Commun. Stat. 3 (1), 1–27, 1974.

Calvo, A.I., Alves, C., Castro, A., Pont, V., Vicente, A.M., Fraile, R., 2013. Research on aerosol sources and chemical composition: past, current and emerging issues. Atmos. Res. 120–121, 1–28. https://doi.org/10.1016/j.atmosres.2012.09.021.

Cappa, C.D., Kolesar, K.R., Zhang, X., Atkinson, D.B., Pekour, M.S., Zaveri, R.A., Zelenyuk, A., Zhang, Q., 2016. Understanding the optical properties of ambient sub- and supermicron particulate matter: results from the CARES 2010 field study in northern California. Atmos. Chem. Phys. 16, 6511–6535. https://doi.org/10.5194/acp-16-6511-2016.

Cazorla, A., Bahadur, R., Suski, K.J., Cahill, J.F., Chand, D., Schmid, B., Ramanathan, V., Prather, K.A., 2013. Relating aerosol absorption due to soot, organic carbon, and dust to emission sources determined from in-situ chemical measurements. Atmos. Chem. Phys. 13, 9337–9350. https://doi.org/10.5194/acp-13-9337-2013.

Diapouli, E., Popovicheva, O., Kistler, M., Vratolis, S., Persiantseva, N., Timofeev, M., Kasper-Giebl, A., Eleftheriadis, K., 2014. Physicochemical characterization of aged biomass burning aerosol after long-range transport to Greece from large scale wildfires in Russia and surrounding regions, Summer 2010. Atmos. Environ. 96, 393–404. https://doi.org/10.1016/j.atmosenv.2014.07.055.

Diémoz, H., Barnaba, F., Ferrero, L., Tombolato, I.K.F., Mapelli, C., Bellini, A., Desandré, C., Magri, T., Zublena, M., 2025. From real-time to long-term source apportionment of PM10 using high-time-resolution measurements of aerosol physical properties: methodology and example application at an urban background site (Aosta, Italy). EGUsphere. https://doi.org/10.5194/egusphere-2025-5044 [Preprint].

Drinovec, L., Močnik, G., Zotter, P., Prévôt, A.S.H., Ruckstuhl, C., Coz, E., Rupakheti, M., Sciare, J., Müller, T., 2015. The “dual-spot” Aethalometer: an improved measurement of aerosol black carbon with real-time loading compensation. Atmos. Meas. Tech. 8, 1965–1979. https://doi.org/10.5194/amt-8-1965-2015.

Ealo, M., Alastuey, A., Ripoll, A., Pérez, N., Minguillón, M.C., Querol, X., Pandolfi, M., 2016. Detection of Saharan dust and biomass burning events using near-real-time intensive aerosol optical properties in the North-Western Mediterranean. Atmos. Chem. Phys. 16, 12567–12586. https://doi.org/10.5194/acp-16-12567-2016.

Everitt, B.S., Landau, S., Leese, M., Stahl, D., 2011. Cluster Analysis. John Wiley & Sons, Ltd.

Forello, A.C., Bernardoni, V., Calzolai, G., Lucarelli, F., Massabò, D., Nava, S., Pileci, R.E., Prati, P., Valentini, S., Valli, G., Vecchi, R., 2019. Exploiting multi-wavelength aerosol absorption coefficients in a multi-time resolution source apportionment study to retrieve source-dependent absorption parameters. Atmos. Chem. Phys. 19, 11235–11252. https://doi.org/10.5194/acp-19-11235-2019.

IPCC, 2023. Climate Change 2023: Synthesis Report. Contribution of Working Groups I, II and III to the Sixth Assessment Report of the Intergovernmental Panel on Climate Change [Core Writing Team, H. Lee and J. Romero (eds.)]. IPCC, Geneva, Switzerland. https://doi.org/10.59327/IPCC/AR6-9789291691647, 184 pp.

Kaskaoutis, D.G., Grivas, G., Stavroulas, I., Liakakou, E., Dumka, U.C., Dimitriou, K., Gerasopoulos, E., Mihalopoulos, N., 2021. In situ identification of aerosol types in Athens, Greece, based on long-term optical and on online chemical characterization. Atmos. Environ. 246, 118070, 1352–2310. https://doi.org/10.1016/j.atmosenv.2020.118070.

Li, W., Shao, L., Zhang, D., Ro, C.U., Hu, M., Bi, X., Geng, H., Matsuki, A., Niu, H., Chen, J., 2016. A review of single aerosol particle studies in the atmosphere of East Asia: morphology, mixing state, source, and heterogeneous reactions. J. Clean. Prod. 112 (2), 1330–1349. https://doi.org/10.1016/j.jclepro.2015.04.050.

Mira-Salama, D., Van Dingenen, R., Gruening, C., Putaud, J.-P., Cavalli, F., Cavalli, P., Erdmann, N., Dell'Acqua, A., Dos Santos, S., Hjorth, J., Raes, F., Jensen, N.R., 2008. Using Föhn conditions to characterize urban and regional sources of particles. Atmos. Res. 90 (2–4), 159–169. https://doi.org/10.1016/j.atmosres.2008.02.007.

Müller, T., Laborde, M., Kassell, G., Wiedensohler, A., 2011. Design and performance of a three wavelength LED-based total scatter and backscatter integrating nephelometer. Atmos. Meas. Tech. 4, 1291–1303. https://doi.org/10.5194/amt-4-1291-2011.

Petzold, A., Ogren, J.A., Fiebig, M., Laj, P., Li, S.-M., Baltensperger, U., Holzer-Popp, T., Kinne, S., Pappalardo, G., Sugimoto, N., Wehrli, C., Wiedensohler, A., Zhang, X.-Y., 2013. Recommendations for reporting "black carbon" measurements. Atmos. Chem. Phys. 13, 8365–8379. https://doi.org/10.5194/acp-13-8365-2013.

Portin, H., Mielonen, T., Leskinen, A., Arola, A., Pärjälä, E., Romakkaniemi, S., Laaksonen, A., Lehtinen, K.E.J., Komppula, M., 2012. Biomass burning aerosols observed in Eastern Finland during the Russian wildfires in summer 2010 – part 1: In-situ aerosol characterization. Atmos. Environ. 47, 269–278. https://doi.org/10.1016/j.atmosenv.2011.10.067.

Rimoldi, S., Acton-Bond, M., Bernardoni, V., Cadeo, L., Valli, G., Colombi, C., Cosenza, R., Manousakas, M.I., Chazeau, B., Vecchi, R., 2026. Atmospheric aerosol light scattering and absorption properties in the urban area of Milan (Italy): a focus on aerosol typing. Atmos. Res. 334, 108776. https://doi.org/10.1016/j.atmosres.2026.108776.

Rivas, I., Beddows, D.C.S., Amato, F., Green, D.C., Järvi, L., Hueglin, C., Reche, C., Timonen, H., Fuller, G.W., Niemi, J.V., Pérez, N., Aurela, M., Hopke, P.K., Alastuey, A., Kulmala, M., Harrison, R.M., Querol, X., Kelly, F.J., 2020. Source apportionment of particle number size distribution in urban background and traffic stations in four European cities. Environ. Int. 135, 105345. https://doi.org/10.1016/j.envint.2019.105345.

Rolph, G., Stein, A., Stunder, B., 2017. Real-time environmental applications and display system: READY. Environ. Model Softw. 95, 210–228. https://doi.org/10.1016/j.envsoft.2017.06.025.

Romano, S., Perrone, M.R., Pavese, G., Esposito, F., Calvello, M., 2019. Optical properties of PM2.5 particles. Results from a monitoring campaign in southeastern Italy. Atmos. Environ. 203, 1352–2310. https://doi.org/10.1016/j.atmosenv.2019.01.037.

Sandradewi, J., Prévôt, A.S.H., Szidat, S., Perron, N., Alfarra, M.R., Lanz, V.A., Weingartner, E., Baltensperger, U., 2008. Using aerosol light absorption measurements for the quantitative determination of wood burning and traffic emission contributions to particulate matter. Environ. Sci. Technol. 42, 3316–3323. https://doi.org/10.1021/es702253m.

Savadkoohi, M., Gherras, M., Favez, O., Petit, J.-E., Rovira, J., Chen, G.I., Via, M., Platt, S., Aurela, M., Chazeau, B., de Brito, J.F., Riffault, V., Eleftheriadis, K., Flentje, H., Gysel-Beer, M., Hueglin, C., Rigler, M., Gregorič, A., Ivančič, M., Keernik, H., Maasikmets, M., Liakakou, E., Stavroulas, I., Luoma, K., Marchand, N., Mihalopoulos, N., Petäjä, T., Prevot, A.S.H., Daellenbach, K.R., Vodička, P., Timonen, H., Tobler, A., Vasilescu, J., Dandocsi, A., Mbengue, S., Vratolis, S., Zografou, O., Chauvigné, A., Hopke, P.K., Querol, X., Alastuey, A., Pandolfi, M., 2025. Addressing the advantages and limitations of using Aethalometer data to determine the optimal absorption Ångström exponents (AAEs) values for eBC source apportionment. Atmos. Environ. 349, 121121. https://doi.org/10.1016/j.atmosenv.2025.121121.

Seinfeld, J.H., Pandis, S.N., 2006. Atmospheric Chemistry and Physics: From Air Pollution to Climate Change, 2nd edition. John Wiley & Sons, New York.

Stein, A.F., Draxler, R.R., Rolph, G.D., Stunder, B.J.B., Cohen, M.D., Ngan, F., 2015. NOAA'S HYSPLIT atmospheric transport and dispersion modelling system. Bull. Am. Meteorol. Soc. 96, 2059–2077. https://doi.org/10.1175/BAMS-D-14-00110.1.

Sumlin, B.J., Pandey, A., Walker, M.J., Pattison, R.S., Williams, B.J., Chakrabarty, R.K., 2017. Atmospheric photooxidation diminishes light absorption by primary brown carbon aerosol from biomass Burnin. Environ. Sci. Technol. Lett. 4 (12), 540–545. https://doi.org/10.1021/acs.estlett.7b00393.

Valentini, S., Barnaba, F., Bernardoni, V., Calzolai, G., Costabile, F., Di Liberto, L., Forello, A.C., Gobbi, G.P., Gualtieri, M., Lucarelli, F., Nava, S., Petralia, E., Valli, G., Wiedensohler, A., Vecchi, R., 2020. Classifying aerosol particles through the combination of optical and physical-chemical properties: results from a wintertime campaign in Rome (Italy). Atmos. Res. 235, 104799. https://doi.org/10.1016/j.atmosres.2019.104799.

Vecchi, R., Marcazzan, G., Valli, G., 2007. A study on nighttime–daytime PM10 concentration and elemental composition in relation to atmospheric dispersion in the urban area of Milan (Italy). Atmos. Environ. 41 (10), 2136–2144, 1352-2310. https://doi.org/10.1016/j.atmosenv.2006.10.069.

Vecchi, R., Piziali, F.A., Valli, G., Favaron, M., Bernardoni, V., 2019. Radon-based estimates of equivalent mixing layer heights: a long-term assessment. Atmos. Environ. 197, 150–158. https://doi.org/10.1016/j.atmosenv.2018.10.020.

WHO Global Air Quality Guidelines, 2021. Particulate matter (PM 2.5 and PM 10), ozone, nitrogen dioxide, sulfur dioxide and carbon monoxide. World Health Organization, Geneva. https://www.who.int/publications/i/item/9789240034228 (accessed on 2/1/2026).

Yus-Dìez, J., Bernardoni, V., Močnik, G., Alastuey, A., Ciniglia, D., Ivančič, M., Querol, X., Perez, N., Reche, C., Rigler, M., Vecchi, R., Valentini, S., Pandolfi, M., 2021. Determination of the multiplescattering correction factor and its cross-sensitivity to scattering and wavelength dependence for different AE33 Aethalometer filter tapes: a multi-instrumental approach. Atmos. Meas. Tech. 14, 6335–6635. https://doi.org/10.5194/amt-14-6335-2021.